Stability Analysis of Hydrodynamic Pressure Landslides with Different Permeability Coefficients Affected by Reservoir Water Level Fluctuations and Rainstorms

Faming Huang [1], Xiaoyan Luo [2] and Weiping Liu [1,*]

[1] School of Civil Engineering and Architecture, Nanchang University, Nanchang 330031, China; huang1503518@sina.cn

[2] School of Civil Engineering and Architecture, Jiangxi Science and Technology Normal University, Nanchang 330013, China; luoxiaoyan2@126.com

* Correspondence: liuweiping@ncu.edu.cn; Tel.: +86-138-7910-1369

Abstract: It is significant to study the variations in the stability coefficients of hydrodynamic pressure landslides with different permeability coefficients affected by reservoir water level fluctuations and rainstorms. The Sifangbei landslide in Three Gorges Reservoir area is used as case study. Its stability coefficients are simulated based on saturated-unsaturated seepage theory and finite element analysis. The operating conditions of stability coefficients calculation are reservoir water level variations between 175 m and 145 m, different rates of reservoir water level fluctuations, and a three-day continuous rainstorm. Results show that the stability coefficient of the hydrodynamic pressure landslide decreases with the drawdown of the reservoir water level, and a rapid drawdown rate leads to a small stability coefficient when the permeability coefficient ranges from 1.16×10^{-6} m/s to 4.64×10^{-5} m/s. Additionally, the landslide stability coefficient increases as the reservoir water level increases, and a rapid increase in the water level leads to a high stability coefficient when the permeability coefficient ranges from 1.16×10^{-6} m/s to 4.64×10^{-5} m/s. The landslide stability coefficient initially decreases and then increases as the reservoir water level declines when the permeability coefficient is greater than 4.64×10^{-5} m/s. Moreover, for structures with the same landslide, the landslide stability coefficient is most sensitive to the change in the rate of reservoir water level drawdown when the permeability coefficient increases from 1.16×10^{-6} m/s to 1.16×10^{-4} m/s. Additionally, the rate of decrease in the stability coefficient increases as the permeability coefficient increases. Finally, the three-day rainstorm leads to a significant reduction in landslide stability, and the rate of decrease in the stability coefficient initially increases and then decreases as the permeability coefficient increases.

Keywords: hydrodynamic pressure landslide; finite element analysis; stability coefficient; permeability coefficient; reservoir water level; rainstorm

1. Introduction

The saturation level and other material properties of reservoir landslides have changed constantly since the impoundment of Three Gorges Reservoir in 2003. Additionally, the hydraulic uplift pressure, hydrostatic pressure and hydrodynamic pressure on the reservoir landslide change periodically due to heavy rainfall and reservoir water level fluctuations [1–5]. Potential landslide instabilities threaten the safety of local residents and property [6–8]. Therefore, it is necessary to explore the change characteristics of landslide stability coefficients under the influences of heavy rainfall and reservoir water level fluctuations.

The landslide permeability coefficients and the mechanism of landslide instability associated with reservoir water level fluctuations are different. Hence, the reservoir landslides in the Three Gorges Reservoir area (TGRA) can be divided into three categories: hydrodynamic pressure landslides, hydraulic uplift pressure landslides and composite landslides [9]. Most of the reservoir landslides in the area are hydrodynamic pressure landslides. The hydrodynamic pressure formed by the water head difference between the landslide groundwater level and the reservoir water level alters the landslide stability coefficient [10]. Additionally, rainfall infiltration increases the landslide groundwater level and decreases the landslide stability coefficient [11,12]. As a result, the seepage field and stability coefficient of a hydrodynamic pressure landslide change significantly due to changes in the reservoir water level, rainfall rate and permeability coefficients [13]. Therefore, it is important to study the seepage fields and characteristics of changes in the stability coefficients of hydrodynamic pressure landslides.

In recent years, many studies of landslide seepage fields and stability coefficients have been performed in the context of reservoir water level fluctuations and heavy rainfall. The groundwater levels and pore water pressures in landslides are affected by the rates of variations in reservoir water levels [14] and by saturated permeability coefficients [15]. As a result, the landslide stability coefficient varies based on changes in the reservoir water level and saturated permeability coefficient [13,16–19]. Notably, some studies have shown that the seepage fields and stability coefficients of reservoir landslides in the TGRA are affected by fluctuations in the reservoir water level [20–24]. Furthermore, Xiang, et al. [25] studied the stability coefficient of a hydrodynamic pressure landslide affected by reservoir water level fluctuations; Chen and Liu [26] studied the seepage field and stability coefficient variations of a reservoir landslide in the TGRA based on different permeability coefficients; and Hsu and Chien [27] studied the landslide stability coefficient under extreme climates. Moreover, Rahimi, et al. [28] found that the saturated permeability coefficient plays an important role in rainfall-induced landslides. However, there is a lack of knowledge regarding the rate of decrease of the stability coefficients of hydrodynamic pressure landslides with different permeability coefficients under the conditions of heavy rainfall and a rapid decline in the reservoir water level.

The saturated-unsaturated seepage theory and finite element analysis have been widely used to analyze changes in the landslide seepage field and stability coefficient. Hu, et al. [29] studied the effects of reservoir water level fluctuations in Three Gorges Reservoir on the stability of Huangtupo Riverside Slumping Mass #II using saturated-unsaturated seepage theory and finite element analysis. Jian, et al. [30] analyzed the seepage field of the Qianjiangping landslide in TGRA at various rainfall rates and reservoir water levels. Song, Yan, Zhang, Lu and Yi [20] studied the effects of the hydraulic properties of the soil and the fluctuation velocity of reservoir water on landslide stability. Chien, et al. [31] used a finite element model to determine the stability coefficients of regional shallow landslides induced by extreme rainfall. In this study, the Sifangbei landslide in the TGRA is used as an example. The seepage field, stability coefficient, and rate of decrease of the stability coefficient of the Sifangbei landslide are studied under different operating conditions based on saturated-unsaturated seepage theory and finite element analysis.

2. Materials

2.1. Engineering Geology

The Sifangbei landslide [32] faces the Yangtze River and exhibits a planar, bush-shaped structure. The landslide has a maximum length of 850 m and maximum width of 400 m and encompasses an area of 34×10^4 m^2. The elevation of the frontal part of the landslide is approximately 125 m, and the elevation of the upper part is approximately 325 m. The mean depth of the sliding surface is approximately 23 m. Hence, the Sifangbei landslide has an estimated volume of 782×10^4 m^3. The left and right boundaries of the landslide are defined by bedrock and a gully, respectively. The upper boundary is defined by the interface between the bedrock and the soil. A topographical map of the landslide is shown in Figure 1.
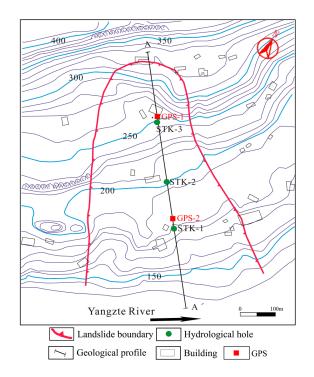
Figure 1. Topographical map of the Sifangbei landslide with the locations of monitoring points.

The geological section A-A′ of the Sifangbei landslide is shown in Figure 2. The landslide is mainly composed of silty clay and fragmented rubble included in a quaternary deposit. The engineering structure is loose and disordered. The formation lithology of the landslide is thick and bedded in Jurassic sandstone, silty mudstones and muddy siltstones. The thickness of the slip zone is approximately 1 m, and it is composed of silty clay and fragmented rubble. The groundwater types of the landslide area are primarily loose debris pore water and bedrock fissure water. In addition, the groundwater levels are mainly affected by the reservoir water level and rainfall.

Figure 2 shows that the morphology of the landslide is characterized by a fold line. The landslide can be divided into an anti-slide section and slide section according to the morphological characteristics of the profile. The slope of the slide surface in the anti-slide section is conservative or adverse; as a result, the resisting sliding force is greater than the driving force in the anti-slide section. However, the slope of slide surface in the slide section is steep; hence, the driving force is greater than the resisting sliding force. The slide mass of the Sifangbei landslide between elevations of 125 m and 145 m is mainly affected by the resisting sliding force, while the slide mass between 145 m and 175 m is mainly affected by the slide force.
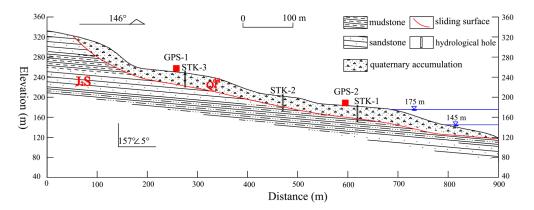

Figure 2. Geological cross-section of the Sifangbei landslide.

2.2. Landslide Deformation Characteristics and Stability Analysis

The Sifangbei landslide has undergone surface deformation since the impoundment of Three Gorges Reservoir. Field investigation shows that surface cracks have mainly occurred at the frontal part of the landslide. These cracks threaten the lives and property of local residents. To monitor the landslide deformation, three groundwater stage gauges, two global positioning system (GPS) points [33,34] and one rain gauge were installed. Point GPS-1 was located on the upper part of the landslide, and point GPS-2 was located on the frontal part of the landslide. Figure 3 shows that the cumulative displacement of GPS-1 was very low at approximately 30 mm, while the cumulative displacement of GPS-2 was very high at approximately 375 mm from April 2007 to December 2009.

Additionally, Figure 3 illustrates that GPS-2 moved relatively slowly from October 2007 to February 2009 but exhibited a high rate of movement from April 2007 to September 2007 and from April 2009 to July 2009. The monitoring values indicated that notable deformation mainly occurred when the reservoir water level declined from 175 m to 145 m, and the displacement rate decreased when the reservoir water level rose from 145 m to 175 m. Hence, the Sifangbei landslide can be considered a hydrodynamic pressure landslide. Moreover, point GPS-2 moved fast during the rainy season each year, indicating that landslide deformation was affected by heavy rainfall. Furthermore, the cumulative displacement of the landslide has increased slowly since October 2009; hence, the landslide has been relatively stable in recent years.
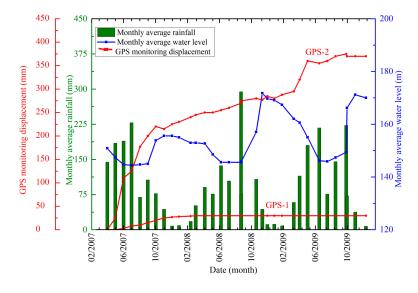

Figure 3. Curves of cumulative landslide displacement monitored by GPS.

3. Methods

3.1. Saturated-Unsaturated Seepage Theory

Changes in the landslide seepage field are significantly influenced by reservoir water level fluctuations and rainfall infiltration. Additionally, saturated and unsaturated zones form through changes in the seepage field. Assuming that pressure head h is the dependent variable in the governing equation, the two-dimensional seepage governing equation can be obtained according to the mass conservation equation and Darcy's law:

$$\frac{\partial}{\partial x}\left(k_x \frac{\partial h}{\partial x}\right) + \frac{\partial}{\partial y}\left(k_y \frac{\partial h}{\partial y}\right) + Q = m_w \rho_w g \frac{\partial h}{\partial t} \tag{1}$$

where t is time; k_x and k_y are the permeability coefficients in the horizontal and vertical directions, respectively; ρ_w is the density of water; g is gravitational acceleration; Q is the boundary discharge;

and m_w is the saturated bulk weight. The variable m_w can be defined as the negative value of the partial derivative of the moisture volume percentage θ_w of matrix suction $(u_\partial - u_w)$:

$$m_w = -\frac{\partial \theta_w}{\partial (u_\partial - u_w)} \tag{2}$$

where u_∂ and u_w are the pore water pressure and pore air pressure, respectively. In addition, m_w can be regarded as the absolute value of the slope of the soil-water characteristic curve (SWCC). The combined seepage governing equation, boundary conditions and initial conditions were used as inputs in the SEEP/W module of Geo-studio 2007 software (Company of GEO-SLOPE, Calgary, AB, Canada) [35] to calculate the seepage field. Then, the SWCC and permeability function curve were obtained. Additionally, the transient seepage field of the landslide can be obtained, and the associated initial condition is defined as follows.

$$h(x, y, 0) = h_0(x, y, 0) \tag{3}$$

The head boundary condition is as follows.

$$k\frac{\partial_h}{\partial_n} = h(x, y, t) \tag{4}$$

The flux boundary condition is given by the following expression.

$$k\frac{\partial_h}{\partial_n}|\gamma_2 = q(x, y, t) \tag{5}$$

In Equations (3)–(5), k is the tensor of the permeability coefficient and n is the unit normal vector of the boundary plane.

3.2. Calculation Theory of the Stability Coefficient

The shear strength theory of unsaturated soil considering a negative pore water pressure is used to calculate the stability coefficient:

$$\tau = c' + (\sigma - u_\partial)\tan \varphi' + (u_\partial - u_w)\tan \varphi^b \tag{6}$$

where c' and φ' are the parameters of the effective stress strength, σ is the total normal stress, u_∂ is the pore air pressure, u_w is the void water pressure, $(u_\partial - u_w)$ is the matrix suction, and φ^b is the increased angle of the strength curve induced by the increase in matrix suction (set as a constant in this study). The current methods used to calculate the landslide stability coefficient considering the matrix suction generally include strength reduction methods and limiting equilibrium methods [36]. Limiting equilibrium methods are widely used and mainly include the Swedish circle method [37], Bishop method [38], Residual thrust method [39] and the Morgenstern-Price (M-P) method [40]. However, the first three stability coefficient calculation methods simplify the interaction force between soil sections; as a result, it is difficult to reflect the actual stress conditions of each soil section. Additionally, the M-P method can determine the stability coefficient of a landslide with any slide surface and reflect the interaction force between the soil sections of the landslide, even for the most dangerous slide surfaces. Therefore, the M-P method is used to calculate the stability coefficient of the Sifangbei landslide.

3.3. Geomechanical Model of the Sifangbei Landslide

The most dangerous geological section is determined according to the engineering geological characteristics of the Sifangbei landslide. In addition, the most dangerous geological section is used to calculate the seepage field and stability coefficient [41]. Two different materials mainly comprise the

geomechanical model: silty clay and fragmented rubble contained in the slide mass and interbedded sandstone and mudstone contained in the ledge rock. The silty clay and fragmented rubble are shown in faint yellow in Figure 4, and the inter-bedded sandstone and mudstone are shown in gray. The anti-slide section in the frontal part of the landslide is submerged at a reservoir water level of 145 m. Therefore, reservoir water level fluctuations mainly affect the slide section in the frontal part of the landslide and have little effect on the anti-slide section.

The slide mass should be divided into many meshes before using 2-dimensional finite element analysis. The mesh size has some impact on the computational precision of the stability coefficient. Some studies show that the computational precision of stability coefficient has an upward tendency and then become stable with the gradually decrease of the mesh size. And also shows that the computational precision and efficiency of stability coefficient will decline when the mesh size is set to a very small value [42]. In this study, the experiment shows that the computational precision of stability coefficient is 0.01 when the mesh size is set to 5 m. Therefore, a mesh size of 5 m is suitable for the finite element analysis of Sifangbei landslide. As shown in Figure 4, 4526 grid cells and 4418 nodes are created using the mesh division method.

To determine the initial groundwater level when the reservoir water level declines from 175 m to 145 m, groundwater levels are measured in the hydrological wells. The average groundwater level depth in STK1 wellis approximately 1.2 m, and the average depth in STK2 well is approximately 2.6 m when the reservoir water level is 175 m without rainfall. In addition, the elevation of the tapping point in the frontal part of the landslide is set at 175 m. Hence, the initial saturation line of the Sifangbei landslide is established as the blue line in Figure 4. Furthermore, to explore the seepage field when the reservoir water level increases from 145 m to 175 m, the stable landslide saturation line of the 145 m reservoir water level is regarded as the initial saturation line.
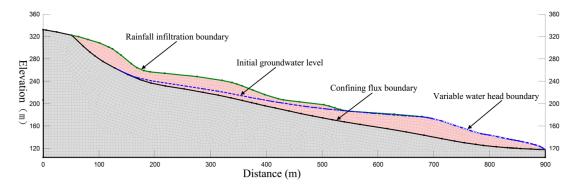

Figure 4. Main sliding section of the landslide.

The mechanical parameters of the slide mass and slide bed are determined as shown in Table 1 based on geological prospecting and laboratory experiments. The material of the slide mass is assumed to have the characteristics of unsaturated soil, and the volumetric water content of the soil and permeability coefficient of the slide mass are functions of the matrix suction when the seepage field is simulated using the SEEP/W module [43].

The soil–water characteristic curve (SWCC) can be used to estimate various parameters used to describe unsaturated soil behavior. It is a relationship between soil suction and some measure of the water content. The volumetric water content and permeability coefficient are constant when the slide mass is in a saturated state. However, they should be determined through laboratory experiments when the slide mass is in an unsaturated state [44]. It is difficult and time-consuming to measure the SWCC for the unsaturated soil using laboratory tests. Therefore, the soil volumetric water content and permeability coefficient are set as empirical model [45]. There are many empirical models used to fit the SWCC, such as the Brooks-Corey model [46], the Gardner model [47], the Van-Genuchten model [48] and the Gardner-Russo model [49]. Among these empirical models, the Van-Genuchten

model is able to obtain a good agreement with the experimental results, and it is applicable for the SWCC measurement of silty clay. Therefore, when simulating the seepage field of Sifangbei landslide, the Van-Genuchten empirical curve in the SEEP/W module and the parameters in the saturated state are used to determine the SWCC of the slide mass as shown in Figure 5.
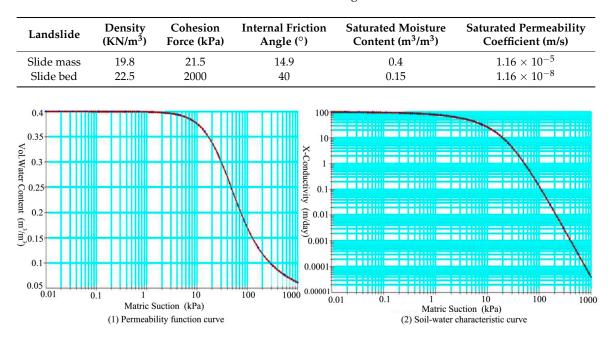
Table 1. Parameters of the Sifangbei landslide.

Landslide	Density (KN/m³)	Cohesion Force (kPa)	Internal Friction Angle (°)	Saturated Moisture Content (m³/m³)	Saturated Permeability Coefficient (m/s)
Slide mass	19.8	21.5	14.9	0.4	1.16×10^{-5}
Slide bed	22.5	2000	40	0.15	1.16×10^{-8}

Figure 5. Soil-water characteristic curve and permeability function of the slide mass.

3.4. Operating Conditions and Boundary Conditions

The rates of increases in the reservoir water level are set to V_{r1} = 0.6 m/d, V_{r2} = 0.9 m/d and V_{r3} = 1.2 m/d, and the corresponding durations are 50 days, 33 days and 25 days, respectively, from 145 m to 175 m. The rates of decreases in the reservoir water level are set to V_{d1} = 0.6 m/d, V_{d2} = 0.9 m/d and V_{d3} = 1.2 m/d. Additionally, the landslide stability coefficients are calculated under the combined operating conditions of a decrease in the reservoir water level of 1.2 m/d and a three-day, heavy rainstorm in the fifty-year return period. The heavy rainstorm occurs when the reservoir water level declines from 161 m to 159 m. The adopted operating conditions are shown in Table 2. In addition, the boundary conditions [20] of all operating conditions are as follows.

(1) The water head boundary condition in the frontal part of the landslide is determined according to the reservoir water level. The landslide surface above the reservoir water level is set as the rainfall infiltration boundary. The elevation of the initial water head is set as 175 m. The reservoir water level between 145 m and 175 m is set as the variable water head boundary condition when the reservoir water level declines from 175 m to 145 m. The bedrock surface is set as the confining flux boundary.

(2) A statistical analysis of daily rainfall data in Wanzhou district from 1960 to 2013 was conducted. The results show that the daily rainfall is R = 90 mm for the three-day heavy rainstorm in the fifty year return period.

Table 2. Different combinations of operating conditions for landslide stability calculations.

Number of Conditions	Continuous Combined Load	Fluctuation Rate of the Reservoir Water Level (m/d)	Rainstorm
1-1	Self-weight+loads on the ground surface+ reservoir water level decline from 175 m to 145 m	0.6 m/d	None
1-2		0.9 m/d	
1-3		1.2 m/d	
2-1	Self-weight+loads on the ground surface+ reservoir water level rise from 145 m to 175 m	0.6 m/d	
2-2		0.9 m/d	
2-3		1.2 m/d	
3-1	Self-weight+loads on the ground surface+ reservoir water level decline from 175 m to 145 m	1.2 m/d	Three-day heavy rainstorm

4. Results and Discussion

4.1. Seepage Field and Stability Coefficient Calculations for the Sifangbei Landslide

4.1.1. Seepage Field Analysis of the Sifangbei Landslide

The seepage fields of the Sifangbei landslide under different operating conditions are calculated. Figure 6 shows that the saturation lines of the landslide decline with the reservoir water level. Additionally, the saturation lines exhibit convex phenomena under the conditions of reservoir water level drawdown, and a hydraulic head difference exists between the landslide groundwater level and the reservoir water level. Moreover, an obvious convex phenomenon can be observed when the rate of decline in the reservoir water level increases.

Figure 7 shows that the landslide saturation lines increase with increasing the reservoir water level. Additionally, a concave phenomenon occurs as the reservoir water level increases, and a more obvious concave phenomenon can be observed when the rate of increase in the reservoir water level increases. Moreover, Figure 8 illustrates that the landslide saturation lines increase quickly when the three-day heavy rainstorm occurs. Then, the saturation lines decrease gradually after the rainstorm stops.
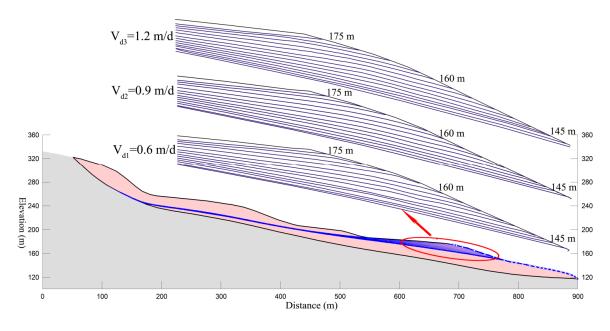

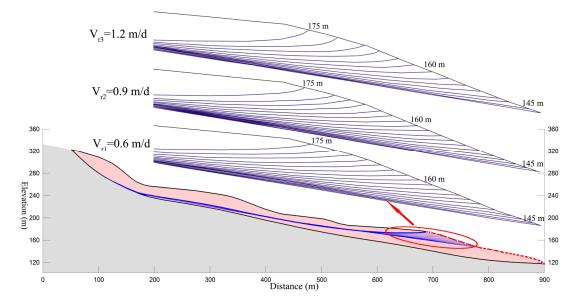**Figure 6.** Transient changes under operating conditions 1-1, 1-2 and 1-3.

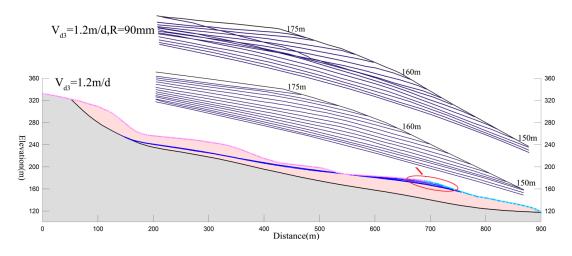**Figure 7.** Transient changes under operating conditions 2-1, 2-2 and 2-3.

Figure 8. Transient changes under operating condition 3.

4.1.2. Stability Coefficient Analysis of the Sifangbei Landslide

The stability coefficients of the Sifangbei landslide under different reservoir water levels of 145 m and 175 m are calculated as shown in Table 3. Table 3 shows that the maximum stability coefficient is 1.254 when the reservoir water level rises to 175 m at a rate of 1.2 m/d. Additionally, the minimum stability coefficient is 1.072 when the reservoir water level declines to 145 m at a rate of 1.2 m/d.

The stability coefficients of the Sifangbei landslide under different operating conditions are shown in Figure 9. Notably, hydrodynamic pressure landslides have some specific response characteristics due to reservoir water level fluctuations. Figure 9(1) shows that the stability coefficient decreases when the reservoir water level declines from 175 m to 145 m. This is because that the decrease in the reservoir water level increases the reverse hydrodynamic pressure on the slide section of the landslide. Meanwhile, the drawdown of the reservoir water level decreases the hydrostatic pressure and the hydraulic uplift pressure on the slide section of the landslide. A large rate of decline in the reservoir water level results in a small landslide stability coefficient because the permeability coefficient of the hydrodynamic pressure landslide is small. As a result, a greater rate of decline in the reservoir water level increases the reverse hydrodynamic pressure and decreases the hydraulic uplift pressure on the landslide.

Figure 9(2) illustrates that the stability coefficient of the Sifangbei landslide increases markedly when the reservoir water level increases. This is because that the increase in the reservoir water level increases the hydrodynamic pressure, the hydrostatic pressure and the hydraulic uplift pressure on the slide section of the landslide. A large rate of increase in the reservoir water level results in a large landslide stability coefficient because it generates a large hydrostatic pressure on the slide section of the landslide. Moreover, Figure 9(3) shows that the stability coefficient decreases markedly in the first few days of the rainstorm. Then, the decrease in the stability coefficient is almost the same as the decrease in the stability coefficient under a reservoir water level drawdown.

Table 3. Stability coefficient at water levels of 145 m and 175 m under different conditions.

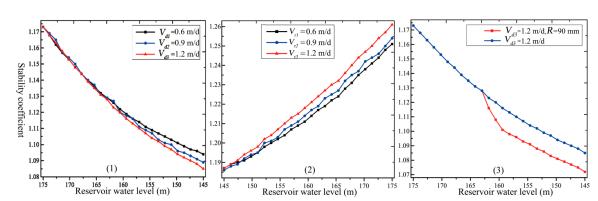| Conditions	1-1	1-2	1-3	2-1	2-2	2-3	3
Water level of 145 m	1.094	1.089	1.085	1.187	1.187	1.187	1.072
Water level of 175 m	1.173	1.173	1.173	1.251	1.254	1.261	1.173

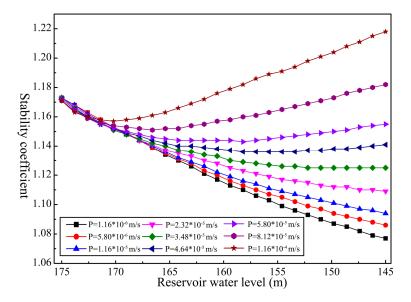**Figure 9.** Stability coefficient of the Sifangbei landslide under different operating conditions.

4.2. Stability Coefficient of the Hydrodynamic Pressure Landslide with Different Permeability Coefficients

The variations in the stability coefficient of the hydrodynamic pressure landslide are explored based on different permeability coefficients and the same geological conditions.

4.2.1. Stability Coefficient Analysis under the Same Rate of Decline in the Reservoir Water Level

First, the permeability coefficients of the Sifangbei landslide are changed to 1.16×10^{-6} m/s (0.1 m/d), 5.8×10^{-5} m/s (0.5 m/d), 1.16×10^{-5} m/s (1 m/d), 2.32×10^{-5} m/s (2 m/d), 3.48×10^{-5} m/s (3 m/d), 4.64×10^{-5} m/s (4 m/d), 5.79×10^{-5} m/s (5 m/d), 8.12×10^{-5} m/s (7 m/d) and 1.16×10^{-4} m/s (10 m/d). Additionally, the rate of decline in the reservoir water level is set to 0.6 m/d. The variations in the stability coefficient of the landslide are shown in Figure 10 for different permeability coefficients. Figure 10 shows that the stability coefficient decreases gradually with the drawdown of the reservoir water level. Additionally, a small permeability coefficient results in a small stability coefficient because the hydrodynamic pressure on the landslide increases as the landslide permeability coefficient decreases when the permeability coefficient ranges from 1.16×10^{-6} m/s to 4.64×10^{-5} m/s. Moreover, Figure 10 illustrates that the landslide stability coefficient initially decreases and then increases with the drawdown of the reservoir water level when the landslide permeability coefficient ranges from 4.64×10^{-5} m/s to 1.16×10^{-4} m/s. These variations occur because the hydrodynamic pressure on the slide section of the landslide decreases rapidly as the reservoir water level declines when the permeability coefficient is large; as result, the slide section is mainly affected by the hydrostatic pressure and the hydraulic uplift pressure. Therefore, although the hydrostatic pressure and the hydraulic uplift pressure decrease when the reservoir water level declines

from 175 m to 145 m, the slide section of the landslide is always affected by the hydrostatic pressure and the hydraulic uplift pressure and not the quickly weakening hydrodynamic pressure.
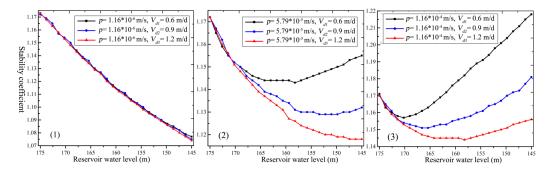

Figure 10. Comparison of stability coefficients for a drawdown rate of 0.6 m/d and different permeability coefficients.

4.2.2. Stability Coefficient Analysis When the Rate of Decline in the Reservoir Water Level Increases

First, the permeability coefficients of the Sifangbei landslide are changed to 1.16×10^{-6} m/s (0.1 m/d), 5.79×10^{-5} m/s (5 m/d) and 1.16×10^{-4} m/s (10 m/d), and the rates of decline in the reservoir water level are changed to V_{d1} = 0.6 m/d, V_{d2} = 0.9 m/d and V_{d3} = 1.2 m/d. Then, the stability coefficients of the landslide are calculated, as shown in Figure 11. Figure 11(1) shows that the stability coefficient decreases considerably with the drawdown of the reservoir water level when the permeability coefficient is 1.16×10^{-6} m/s. However, the ranges of variations in the stability coefficient are small for various rates of decline in the reservoir water level because the permeability coefficient of the landslide is small; as a result, although the hydrodynamic pressure on the slide section increases with the drawdown of the reservoir water level, the hydraulic uplift pressure on the slide section slowly decreases.

The landslide stability coefficient for a permeability coefficient of 5.79×10^{-5} m/s is shown in Figure 11(2). Figure 11(2) illustrates that the landslide stability coefficient initially decreases. Then, the coefficient increases when the rate of decline in the reservoir water level is 0.6 m/d. This is because the landslide permeability coefficient is relatively large; thus, the hydrodynamic pressure caused by the drawdown of the reservoir water level is small. However, the hydrodynamic pressure is still greater than the hydrostatic pressure and the hydraulic uplift pressure when the reservoir water level declines from 175 m to 165 m. Moreover, the hydrostatic pressure and the hydraulic uplift pressure are greater than the hydrodynamic pressure when the reservoir water level declines from 165 m to 145 m. In addition, the landslide is affected by a larger hydrodynamic pressure when the rate of decline in the reservoir water level is 0.9 m/d; as a result, the landslide stability coefficient decreases when the reservoir water level declines from 175 m to 155 m. Then, the landslide stability coefficient increases when the reservoir water level declines from 155 m to 145 m. Furthermore, the landslide stability coefficient is small and declines gradually when the rate of decline in the reservoir water level is 1.2 m/d. Figure 11(2) illustrates that the landslide stability coefficient markedly changes with different rates of decline in the reservoir water level when the permeability coefficient is 5.79×10^{-5} m/s. Additionally, Figure 11(3) shows that the landslide stability coefficient decreases in the initial stage and then rapidly increases when the permeability coefficient is 1.16×10^{-4} m/s.

Figure 11. Comparison of the stability coefficient and water level drawdown for different permeability coefficients.

It is important to study the variations in the stability coefficient of the hydrodynamic pressure landslide for different permeability coefficients and increases in the rate of decline in the reservoir water level. In this study, the rate of decrease of the stability coefficient (*RDSC*) is used [20]. *RDSC* donates the rate of decrease in the stability coefficient of a hydrodynamic pressure landslide for a certain permeability coefficient when the rate of drawdown of the reservoir water level changes from 0.6 m/d to 1.2 m/d. A large *RDSC* value suggests that the *RDSC* increases the rate of drawdown of the reservoir water level increases. *RDSC* can be expressed as follows:

$$RDSC = \frac{F(P, V_d = 0.6 \text{ m/d}, H = 145 \text{ m}) - F(P, V_d = 1.2 \text{ m/d}, H = 145 \text{ m})}{F(P, V_d = 0.6 \text{ m/d}, H = 145 \text{ m})} \tag{7}$$

where *P* is the permeability coefficient, *H* is the reservoir water level, and *F()* is the landslide stability coefficient based on different permeability coefficients and rates of reservoir water level decline and a reservoir water level of 145 m.

The *RDSC* of the Sifangbei landslide is calculated for permeability coefficients of 1.16×10^{-6} m/s (0.1 m/d), 5.79×10^{-6} m/s (0.5 m/d), 1.16×10^{-5} m/s (1 m/d), . . . , and 1.16×10^{-4} m/s (10 m/d). The calculated *RDSC* values are shown in Figure 12. For the hydrodynamic pressure landslide under the condition of reservoir water level drawdown, a large permeability coefficient is associated with a large *RDSC* value when the rate of reservoir water level drawdown changes from 0.6 m/d to 1.2 m/d. A large *RDSC* value is observed because the landslide seepage field is affected by the increase in the rate of reservoir water level decline when the landslide permeability coefficient is relatively large. Moreover, the landslide seepage field is slightly affected by increasing the rate of decline in the reservoir water level when the landslide permeability coefficient is relatively small.
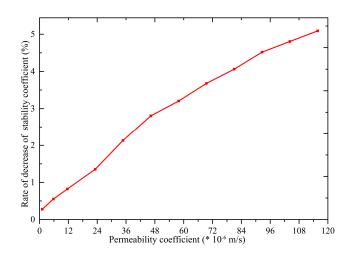

Figure 12. *RDSC* for water level drawdown at different speeds.

4.2.3. Stability Coefficient Variations under Rainstorm Conditions

In this section, the *RDSC* is used to explore the variations in the stability coefficient of the hydrodynamic pressure landslide based on different permeability coefficients when the landslide is affected by a heavy rainstorm. A large *RDSC* value suggests that the decrease in the landslide stability coefficient is large under heavy rainstorm conditions. This relationship can be expressed as follows:

$$RDSC = \frac{F(P, V_d = 1.2 \text{ m/d}, H = 158.2 \text{ m}, R) - F(P, V_d = 1.2 \text{ m/d}, H = 158.2 \text{ m})}{F(P, V_d = 1.2 \text{ m/d}, H = 158.2 \text{ m})} \tag{8}$$

where R is the three-day rainstorm. The permeability coefficients of the Sifangbei landslide are set to 1.16×10^{-6} m/s, 5.79×10^{-6} m/s, ..., and 1.16×10^{-4} m/s. The calculated *RDSC* values are shown in Figure 13. For the hydrodynamic pressure landslide influenced by reservoir water level drawdown, the *RDSC* values increase as the permeability coefficient increases from 1.16×10^{-6} m/s to 3.48×10^{-5} m/s when the landslide is affected by the rainstorm. This increase occurs because rainfall infiltration increases with the landslide permeability coefficient, which ranges from 1.16×10^{-6} m/s to 3.48×10^{-5} m/s when the landslide is affected by the rainstorm; as a result, the hydrodynamic pressure on the landslide increases. Additionally, Figure 13 shows that the *RDSC* decreases with the permeability coefficient ranging from 3.48×10^{-5} m/s to 1.16×10^{-4} m/s when the landslide is affected by the rainstorm. This decrease occurs because the infiltrated rainfall quickly flows through the landslide when the permeability coefficient varies between 3.48×10^{-5} m/s and 1.16×10^{-4} m/s; as a result, the hydrodynamic pressure on the landslide is small, although the landslide is affected by the rainstorm.
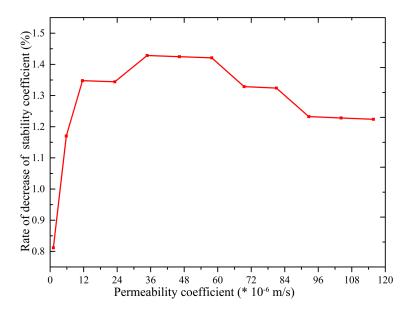

Figure 13. *RDSC* for different permeability coefficients under rainstorm conditions.

5. Conclusions

1) For landslide permeability coefficients ranging from 1.16×10^{-6} m/s to 4.64×10^{-5} m/s, the landslide stability coefficient decreases significantly with the drawdown of the reservoir water level. Additionally, a large rate of decline in the reservoir water level results in a small landslide stability coefficient. Moreover, the landslide stability coefficient significantly increases with the reservoir water level, and a large rate of increase in the reservoir water level results in a large landslide stability coefficient.

2) When the landslide permeability coefficient is greater than the 4.64×10^{-5} m/s, the hydrodynamic pressure on the landslide decreases and the hydraulic uplift pressure increases; as a result, the

stability coefficient initially decreases and then increases with the drawdown of the reservoir water level. Thus, a large rate of decline in the reservoir water level results in a small landslide stability coefficient.

3) For the hydrodynamic pressure landslide with different permeability coefficients, the rate of decline in the reservoir water level varies from 0.6 m/d to 1.2 m/d. As a result, the *RDSC* of the landslide increases gradually as the landslide permeability coefficient increases. In addition, when the landslide is influenced by reservoir water level drawdown and a three-day rainstorm, the *RDSC* increases as the permeability coefficient increases from 1.16×10^{-6} m/s to 3.48×10^{-5} m/s. Then, the *RDSC* decreases as the permeability coefficient increases from 3.48×10^{-5} m/s to 1.16×10^{-4} m/s.

Conflicts of Interest: The authors declare no conflict of interest.

References

1. Min, X.; Ren, G.M.; Lei, X. Deformation and mechanism of landslide influenced by the effects of reservoir water and rainfall, three gorges, China. *Nat. Hazard.* **2013**, *68*, 467–482.
2. Huang, F.; Yin, K.; He, T.; Zhou, C.; Zhang, J. Influencing factor analysis and displacement prediction in reservoir landslides—A case study of Three Gorges Reservoir (China). *Tehnički Vjesnik* **2016**, *23*, 617–626.
3. Huang, F.; Yin, K.; Huang, J.; Gui, L.; Wang, P. Landslide susceptibility mapping based on self-organizing-map network and extreme learning machine. *Eng. Geol.* **2017**, *223*, 11–22. [CrossRef]
4. Chen, C.Y.; Chen, L.K.; Yu, F.C.; Lin, S.C.; Lin, Y.C.; Lee, C.L.; Wang, Y.T. Landslides affecting sedimentary characteristics of reservoir basin. *Environ. Earth Sci.* **2010**, *59*, 1693–1702. [CrossRef]
5. Huang, F.; Huang, J.; Jiang, S.; Zhou, C. Landslide displacement prediction based on multivariate chaotic model and extreme learning machine. *Eng. Geol.* **2017**, *218*, 173–186. [CrossRef]
6. Kwon, T.H.; Cho, G.C. Submarine slope failure primed and triggered by bottom water warming in oceanic hydrate-bearing deposits. *Energies* **2012**, *5*, 2849–2873. [CrossRef]
7. Caloiero, T.; Pasqua, A.A.; Petrucci, O. Damaging hydrogeological events: A procedure for the assessment of severity levels and an application to Calabria (Southern Italy). *Water* **2014**, *6*, 3652–3670. [CrossRef]
8. Chang, C.H.; Harrison, J.F.; Huang, Y.C. Modeling typhoon-induced alterations on river sediment transport and turbidity based on dynamic landslide inventories: Gaoping river basin, Taiwan. *Water* **2015**, *7*, 6910–6930. [CrossRef]
9. Xiao, S.; Hu, Z.; Lu, S.; Ming, C.; Chen, D. Classification of reservoir-triggered landsldies in Three Gorges Reservoir area. *J. Yangzte River Sci. Res. Inst.* **2013**, *30*, 39–44.
10. Peng, R.; Hou, Y.; Zhan, L.; Yao, Y. Back-analyses of landfill instability induced by high water level: Case study of shenzhen landfill. *Int. J. Environ. Res. Public Health* **2016**, *13*, 126. [CrossRef] [PubMed]
11. Cao, C.; Wang, Q.; Chen, J.; Ruan, Y.; Zheng, L.; Song, S.; Niu, C. Landslide susceptibility mapping in vertical distribution law of precipitation area: Case of the xulong hydropower station reservoir, Southwestern China. *Water* **2016**, *8*, 270. [CrossRef]
12. Huang, F.; Huang, J.; Jiang, S.; Zhou, C. Groundwater levels prediction using evidence of chaos and support vector machine. *J. Hydroinf.* **2017**, *19*. [CrossRef]
13. He, K.; Li, X.; Yan, X.; Guo, D. The landslides in the Three Gorges Reservoir region, China and the effects of water storage and rain on their stability. *Environ. Geol.* **2008**, *55*, 55–63.
14. Yan, Z.-L.; Wang, J.-J.; Chai, H.-J. Influence of water level fluctuation on phreatic line in silty soil model slope. *Eng. Geol.* **2010**, *113*, 90–98. [CrossRef]
15. Deng, J.; Wei, J.; Min, H.; Tham, L.; Lee, C. Response of an old landslide to reservoir filling: A case history. *Sci. China Ser. E* **2005**, *48*, 27–32.

16. Berilgen, M.M. Investigation of stability of slopes under drawdown conditions. *Comput. Geotech.* **2007**, *34*, 81–91. [CrossRef]

17. Luo, X.; Sun, H.; Tham, L.; Junaideen, S. Landslide model test system and its application on the study of shiliushubao landslide in Three Gorges Reservoir area. *Soils Found.* **2010**, *50*, 309–317. [CrossRef]

18. Cojean, R.; Caï, Y.J. Analysis and modeling of slope stability in the Three-Gorges Dam reservoir (China)—The case of Huangtupo landslide. *J. Mt. Sci.* **2011**, *8*, 166–175. [CrossRef]

19. Paronuzzi, P.; Rigo, E.; Bolla, A. Influence of filling–drawdown cycles of the Vajont reservoir on Mt. Toc slope stability. *Geomorphology* **2013**, *191*, 75–93. [CrossRef]

20. Song, K.; Yan, E.; Zhang, G.; Lu, S.; Yi, Q. Effect of hydraulic properties of soil and fluctuation velocity of reservoir water on landslide stability. *Environ. Earth Sci.* **2015**, *74*, 5319–5329. [CrossRef]

21. Xu, W.; Wang, L.; Hu, R. Fluid-solid coupling characteristics and stability analysis of soil-rock mixture slope in rising and drawdown of reservoir water levels. *Chin. J. Rock Mech. Eng.* **2009**, *28*, 1491–1498.

22. Liao, H.-J.; Sheng, Q.; Gao, S.-H.; Xu, Z.-P. Influence of drawdown of reservoir water level on landslide stability. *Yanshilixue Yu Gongcheng Xuebao/Chin. J. Rock Mech. Eng.* **2005**, *24*, 3454–3458.

23. Liu, X.-X.; Xia, Y.-Y.; Lian, C.; Zhang, K.-P. Research on method of landslide stability valuation during sudden drawdown of reservoir level. *Rock Soil Mech. Wuhan* **2005**, *26*, 1427–1431.

24. Ding, X.; Fu, J.; Zhang, Q. Stability analysis of landslide in the south end of fengjie highway bridge with fluctuation of water level of Three Gorges Reservoir. *Chin. J. Rock Mech. Eng.* **2004**, *17*, 2913–2919.

25. Xiang, L.; Wang, S.; Wang, L. Response of hydrodynamic pressure landslide to reservoir water level fluctuation: Shuping landslide in Three Gorges Reservoir as an example. *J. Eng. Geol.* **2014**, *22*, 876–882.

26. Chen, S.; Liu, Q. The unsaturated seepage analysis for the influence of water level fluctuation to the pore water pressure of landslide in reservoir area. *Highw. Eng.* **2008**, *33*, 55–59.

27. Hsu, C.F.; Chien, L.K. Slope stability analysis of transient seepage under extreme climates: Case study of typhoon Nari in 2001. *J. Mar. Sci. Technol.* **2016**, *24*, 399–412.

28. Rahimi, A.; Rahardjo, H.; Leong, E.-C. Effect of hydraulic properties of soil on rainfall-induced slope failure. *Eng. Geol.* **2010**, *114*, 135–143. [CrossRef]

29. Hu, X.; Tang, H.; Li, C.; Sun, R. Stability of huangtupo riverside slumping mass II# under water level fluctuation of Three Gorges Reservoir. *J. Earth Sci.* **2012**, *23*, 326–334.

30. Jian, W.; Xu, Q.; Yang, H.; Wang, F. Mechanism and failure process of qianjiangping landslide in the Three Gorges Reservoir, China. *Environ. Earth Sci.* **2014**, *72*, 2999–3013. [CrossRef]

31. Chien, L.K.; Hsu, C.F.; Yin, L.C. Warning model for shallow landslides induced by extreme rainfall. *Water* **2015**, *7*, 4362–4384. [CrossRef]

32. Du, X. The rescarch and application of distortion correction method to landslide physical simulation. *J. Changchun Inst. Technol.* **2013**, *1*, 15–18.

33. Koch, F.; Schlenz, F.; Prasch, M.; Appel, F.; Ruf, T.; Mauser, W. Soil moisture retrieval based on GPS signal strength attenuation. *Water* **2016**, *8*, 276. [CrossRef]

34. Huang, F.M.; Wu, P.; Ziggah, Y.Y. GPS monitoring landslide deformation signal processing using time-series model. *Int. J. Signal Process. Image Process. Pattern Recognit.* **2016**, *9*, 321–332. [CrossRef]

35. Raj, M.; Sengupta, A. Rain-triggered slope failure of the railway embankment at Malda, India. *Acta Geotech.* **2014**, *9*, 789–798. [CrossRef]

36. Kalenchuk, K.; Hutchinson, D.; Diederichs, M. Downie slide: Numerical simulation of groundwater fluctuations influencing the behaviour of a massive landslide. *Bull. Eng. Geol. Environ.* **2013**, *72*, 397–412. [CrossRef]

37. Flaate, K.; Preber, T. Stability of road embankments in soft clay. *Can. Geotech. J.* **1974**, *11*, 72–88. [CrossRef]

38. Bishop, A.; Morgenstern, N. Stability coefficients for earth slopes. *Geotechnique* **1960**, *10*, 129–153. [CrossRef]

39. Luo, L.-J.; Zhao, F.-S.; Hu, J.-Y.; Wang, H. Reliability of high loess slope stability based on residual thrust method. *J. Chang'an Univ.* **2008**, *28*, 27–31.

40. Fredlund, D.; Krahn, J. Comparison of slope stability methods of analysis. *Can. Geotech. J.* **1977**, *14*, 429–439. [CrossRef]

41. Tang, H.; Li, C.; Hu, X.; Su, A.; Wang, L.; Wu, Y. Evolution characteristics of the huangtupo landslide based on in situ tunneling and monitoring. *Landslides* **2015**, *12*, 511–521. [CrossRef]

42. Nam, J.W.; Kim, J.-H.J.; Kim, S.B.; Yi, N.H.; Byun, K.J. A study on mesh size dependency of finite element blast structural analysis induced by non-uniform pressure distribution from high explosive blast wave. *KSCE J. Civ. Eng.* **2008**, *12*, 259–265. [CrossRef]

43. Yeh, H.F.; Wang, J.; Shen, K.L.; Lee, C.H. Rainfall characteristics for anisotropic conductivity of unsaturated soil slopes. *Environ. Earth Sci.* **2015**, *73*, 8669–8681. [CrossRef]

44. Elkady, T.Y.; Almahbashi, A.; Dafalla, M.; Alshamrani, M. Effect of compaction state on the soil water characteristic curves of sand–natural expansive clay mixtures. *Eur. J. Environ. Civ. Eng.* **2017**, *21*, 289–302. [CrossRef]

45. Navid, G.; Pisheh, Y.P. Prediction of soil-water characteristic curve based on soil index properties. In *Experimental Unsaturated Soil Mechanics*; Springer: Berlin, Germany, 2010; pp. 355–367.

46. Milly, P.C.D. Estimation of brooks-corey parameters from water retention data. *Water Resour. Res.* **1987**, *23*, 1085–1089. [CrossRef]

47. Gardner, W.R.; Hillel, D.; Benyamini, Y. Post-irrigation movement of soil water: 2. Simultaneous redistribution and evaporation. *Water Resour. Res.* **1970**, *6*, 1148–1153. [CrossRef]

48. Genuchten, M.T.V. A closed-form equation for predicting the hydraulic conductivity of unsaturated soils. *Soil Sci. Soc. Am. J.* **1980**, *44*, 892–898. [CrossRef]

49. Russo, D. Determining soil hydraulic properties by parameter estimation: On the selection of a model for the hydraulic properties. *Water Resour. Res.* **1988**, *24*, 453–459. [CrossRef]